Journal of Magnetism and Magnetic Materials 517 (2021) 167369

Contents lists available at ScienceDirect

Journal of Magnetism and Magnetic Materials

journal homepage: www.elsevier.com/locate/jmmm

Research articles

Analyses and verifications of magnetic shielding of long pipelines aiming for pipeline orientation measurements

Huang Xinjing[a,b], Li Zan[a,b], Zhang Yu[a,b,*], Xue Yameng[a,b], Li Jian[a,b]

[a] State Key Laboratory of Precision Measuring Technology and Instruments, Tianjin University, Tianjin 300072, People's Republic of China
[b] Binhai International Advanced Structural Integrity Research Centre, Tianjin 300072, People's Republic of China

So far, none of conventional magnetic shielding models can model a field long pipeline consisting of many welded short sections with different permeabilities. This paper demonstrates the magnetic shielding model of long pipelines via simulation analyses based on the finite element method (FEM) and experimental verifications of the magnetic shielding of short pipes, torus pipes, and field long pipelines. The radial and axial shielding factors of a finite pipe can be accurately calculated by the FEM. As the pipe length increases, the axial factor rapidly converges to a value less than 1, and the convergence value is independent of the pipe length because of the magnetic charges at the two ends. For a long pipeline consisting of many short sections, the averaged shielding factors over a couple of adjacent sections are equal to that of an ideal infinite pipeline, and the axial factor is always equal to 1. An "average" strategy for field pipeline orientations that employs the averaged magnetic fields and shielding factors over several sections is then proposed and demonstrated. As the geomagnetic field is taken as the absolute reference, this orientation measurement method has no risk of divergence over a long time and distance.

Index Terms—cylindrical magnetic shield, magnetic fields, pipeline orientation.

1. Introduction

Ferromagnetic thin shells with high magnetic permeability are often employed for reducing the magnetic flux density in a confined region in order to be compliant with acceptable maximum levels for persons or devices [1–4], which is well known and called passive magnetic shielding [56]. Cylindrical shields are often used because they satisfy the symmetry requirement and are relatively easy to manufacture.

1.1. Related Works

Exact solutions of the fields inside the shields are required for multi-layered shields, in order to obtain the maximum magnetic shielding effectiveness with a compact enough structure [7–9], by optimizing geometric dimensions, such as the ratio of shield length to radius, radial spacing, wall thickness. However, exact solutions for both axial and radial orientations only exist for infinite cylinders or spheres. The magnetic fields inside a finite cylindrical shield, which is practical, realizable, and most widely used, can only be approximately solved [10–13]. One such approximation uses the "demagnetizing" factor of an ellipsoid with appropriate radii, where the cylinder is approximated by the ellipsoid [1415]. This approximation is only valid for a limited range of geometric parameters.

Another case for which the magnetic shielding needs to be exactly modeled is low-cost, quasi-real-time inner magnetic inspections of pipelines [16], including utilizing the magnetic fields inside the long pipelines to measure pipeline orientations. The amplitude and direction of the geomagnetic field in the local area are constant. The axial and radial components of the magnetic fields inside the pipelines are determined by the resultants between the orientations of the pipeline and the geomagnetic field, and the magnetic shielding model of the pipeline [1718]. The measured internal magnetic fields can be employed to calculate the pipeline orientations; The orientation accuracy depends on not only the magnetic measurement accuracy, but also the validity of the magnetic shielding model that is quantitatively described by the radial and axial shielding factors.

1.2. Motivation and Technical Challenge

The magnetic shielding of long pipelines has not been modeled yet because any long oil/gas/water pipeline consists of many welded short sections, whose magnetic shielding effects are randomly distributed, relatively independent, and mutually influential. On one hand, field pipelines are very long, usually several or even tens of kilometers, and it is reasonable for them to be considered infinitely long. On the other hand, each section is of finite length and has various magnetic

* Corresponding author.
E-mail address: zhangyu@tju.edu.cn (Z. Yu).

https://doi.org/10.1016/j.jmmm.2020.167369
Received 29 July 2020; Received in revised form 18 August 2020; Accepted 26 August 2020
Available online 10 September 2020
0304-8853/

permeabilities and/or permeability distributions. The pipeline steel has unpredictable complicated original magnetizations at different parts, imprinted during molding and being changed by physical stresses while being forged and further thermal treatment processes. Under the action of the hysteresis and magneto-mechanical effects, the traditional ideal magnetic shielding models are incapable of describing the magnetic fields inside the pipeline.

Before the internal magnetic fields can be utilized to calculate the pipeline orientations, three issues must be addressed: (i) Whether the magnetic shielding of the pipeline complies with the ideal infinite model or the finite model; (ii) How to accurately calculate and obtain the shielding factors of the long pipelines; (iii) How to implement magnetic measurements of pipeline orientations. This work will answer the three questions via simulation analyses based on the finite element method (FEM) and experimental verifications of the magnetic shielding of short sections, torus pipes, and field long pipelines aiming at pipeline orientation measurements.

2. Key Contributions

This is the first time that magnetic shielding of long pipelines aiming for pipeline orientation measurements is analyzed and verified. Conventional magnetic shielding models mostly focus on the design of large magnetic shielding efficiency, and none of them can model the magnetic shielding of a field long pipeline consisting of many welded short sections with different permeabilities. They either considers the pipe to be infinitely long or considers the pipe to be finitely long; but both considerations utilize a uniform magnetic permeability distribution. The new key contributions of this paper are as follows:

1) The FEM is demonstrated to be capable of accurately calculating both the axial and radial magnetic shielding factors of a pipe without any approximation for an explicit permeability. The infinite pipe model (IPM) can only correctly calculate the radial factor while the ellipsoid model (EM) can neither.
2) The FEM is then employed to calculate the shielding factors of torus pipes with random permeability distributions that are proposed to mimic field infinite pipelines that have no start and end but have uneven and unpredictable original magnetizations. It is demonstrated that the averaged shielding factors of an infinite pipeline consisting of many sections are equal to that of an infinite pipeline with the average permeability of those sections.
3) An “average” strategy for magnetic measurements of field pipeline orientations is then proposed. The pipeline orientations can be correctly calculated by using the averaged magnetic fields and the averaged shielding factors over several sections. As the geomagnetic field is taken as the absolute reference, this orientation method has no risk of divergence over a long time and distance.

1.4. Paper Organization

First, FEM is used to study the radial and axial magnetic shield factors of short pipes and long pipelines consisting many sections. Two classical conventional models are briefly introduced: the EM and the IPM, to select the sweeping the dependent variables of magnetic shielding in simulations. Simulations based on the FEM for short pipes and torus pipes are carried out. The torus pipes without ends are used to mimic infinite pipelines. Second, the simulation results are experimentally validated by measuring the shielding factors of a couple of pipes of various sizes. The shielding model of long pipelines is also determined at the same time after the simulations are validated. Third, the shielding model of a long pipeline and its field application are demonstrated via magnetic measurements inside a long field pipeline by using an internal spherical detector (SD) [19–22].

2. FEM-based analyses and verifications

FEM-based simulations have three roles in this paper: First, they are used to justify the use of small pipes in the following experiments to mimic large pipes on site; Second, they are used to compare with the classical magnetic shielding models and experimental results in order to verify the correctness of the simulation results and the applicability of each model in describing the magnetic shielding model of long pipelines; Third, they can explain why increasing the pipe length cannot make the axial shielding factor of one section of pipe converge to 1 due to the surface and volume magnetic charge densities at the two ends of the pipe.

2.1. Selection of Dependent Variables of Magnetic Shielding Factors

The magnetic shielding factors are defined as the ratio of the internal magnetic flux density B_1 and the ambient magnetic flux density B_0:

$$\lambda_i = B_{1i}/B_{0i}, \quad (1)$$

where $i = r$ or a, denoting radial or axial component. The EM and the IPM are two classical models to formulize the shielding factors. These two models utilize many simplifications and are therefore inaccurate, but can be used to qualitatively determine the parameters that determine the magnetic shielding factors. These parameters are key examination objects in the following FEM based simulations.

The EM is for pipes with arbitrary finite lengths [1415]. The axial shielding factor of a single-layer cylinder can be calculated by approximating it to an ellipsoid with its major and minor axes equal to the length L and the diameter D of the cylinder, respectively. Assume that $T=L/D$, the pipe wall thickness is d, the relative magnetic permeability of the material is μ_r, and the ellipsoidal shell is magnetized by an external magnetic field. The shielding factors along the axial and radial directions are

$$\lambda_a = \frac{1}{1+\mu_r \frac{4d}{D} N_a}, \quad (2)$$

and

$$\lambda_r = \frac{1}{1+\mu_r \frac{2d}{D}[1+T^{-2}]N_r}, \quad (3)$$

where

$$N_a = \frac{1}{T^2-1}\left[\frac{T}{\sqrt{T^2-1}} \ln\left(T+\sqrt{T^2-1}\right) - 1\right], \quad (4)$$

and

$$N_r = \frac{1}{2}(1-N_a)\frac{4}{\pi}. \quad (5)$$

The IPM asserts infinite pipes have no shielding effect in the axial direction, namely, $\lambda_a = 1$, and the radial shielding factor is as Eq.(6) [23]. An oil/gas/water pipeline can be assumed to be infinite relative to its diameter, so the cylindrical infinite cavity model can possibly characterize its shielding effectiveness, which needs numerically or experimentally verified.

$$\lambda_r = \frac{4\mu_r p}{(\mu_r^2+1)(p-1)+2\mu_r(p+1)} \approx \frac{4p}{\mu_r(p-1)+2(p+1)} \quad when\ \mu_r >> 1 \quad (6)$$

where $p = \frac{(R+d)^2}{R^2}$ and $R=D/2$.

The two classic models above indicate that the magnetic shielding factors of pipes are determined by several parameters such as the pipe diameter D, the wall thickness d, the length L, and the magnetic permeability μ_r. The length of one section of the industrial pipeline is fixed and about 12 meters limited by transport capacity, and the diameter is 6~40 inches with an incremental step of 2 inches. Therefore, length to diameter ratio (LDR) L/D is about 12~80. Thickness of an industrial pipeline is also discrete and is determined by the standard dimensional ratio (SDR), which is defined as the ratio of pipeline diameter to thickness. There is a series of limited standard values for industrial pipelines, such as SDR11, SDR13.6, SDR17, SDR21, SDR26, and SDR33. Steels used for manufacturing industrial pipelines are chosen from the following series: ASME-SA-515GR, ASME-SA-285, ASME-SA-516GR, API-SPEC-5L-X42, API-SPEC-5L-X60, API-SPEC-5L-X70, and so on. All of them belong to low carbon structural steel family, whose permeability at low ambient fields 0~100 μT is 50~600 [24]. The magnetic field measurement experiments inside the pipeline also confirmed that

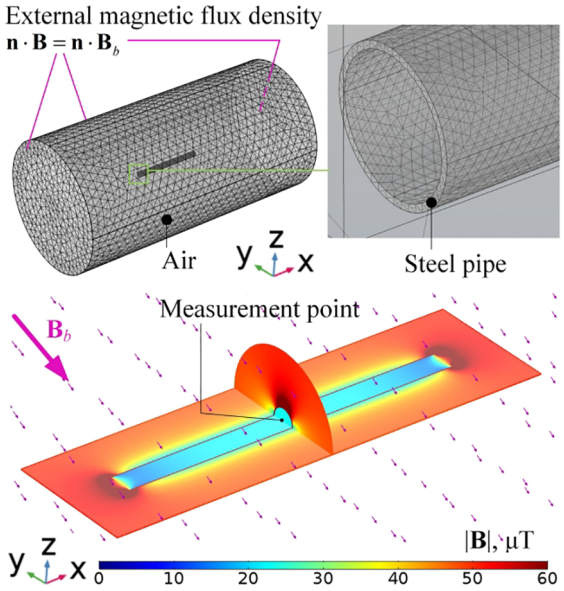

Fig. 1. Simulation model and measurement point

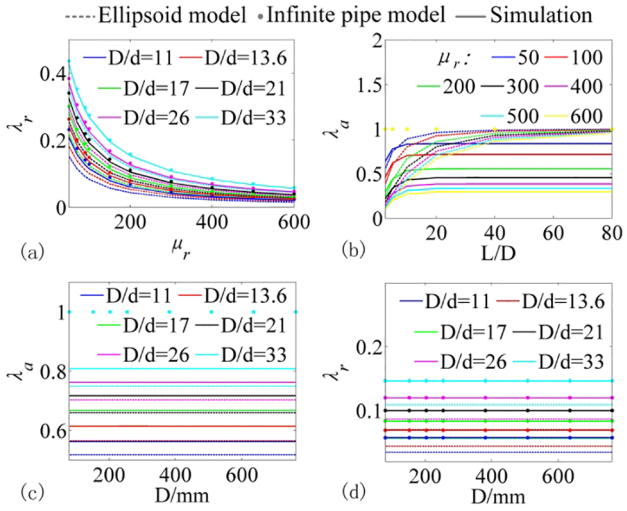

Fig. 2. Magnetic shielding factors for finite pipes, calculated by three methods: EM (dashed lines), IPM (dots), and FEM (solid lines). (a) λ_r vs μ_r for different D/d; (b) λ_a vs L/D for different μ_r; (c) λ_a vs D for different D/d; (d) λ_r vs D for different D/d.

the permeability of the pipeline is 100~200.

2.2. Single-section Pipes with Different Specifications

The finite element simulation software COMSOL is used to sweep these parameters and calculate the axial and radial magnetic shielding factors, λ_a and λ_r, of finite straight pipes with various lengths, to compare with and verify the above two models. The "*Magnetic Fields, No Currents*" interface of AC/DC Module in COMSOL is employed. The formulation used is stationary in 3D. The physics interface formulates and solves Gauss' Law for the magnetic field using the scalar magnetic potential as the dependent variable. This is a magnetostatic problem where no electric currents are present, so you have $\nabla \times H = 0$. This implies that the magnetic scalar potential V_m can be defined from the relation $H = -\nabla V_m$, which is analogous to the definition of the electric potential for static electric fields. Using the constitutive relation $B = \mu_0(H + M)$, the equation $\nabla \cdot B = 0$ becomes

$$-\nabla \cdot (\mu_0 \nabla V_m - \mu_0 M) = 0. \quad (7)$$

The *Magnetic Flux Conservation* node adds Eq. (7) above for the magnetic potential and provides an interface for defining the constitutive relation and the relative permeability μ_r.

As shown in Fig. 1, a steel pipe with permeability of μ_r is submerged in an air domain with a permeability of 1. The pipe axis is parallel to the x axis. The outer surfaces of the air domain are set as the *External Magnetic Flux Density* boundary condition to force the total field to be equal to the background field on the external boundaries. The air domain is much larger than the pipe domain to make the external boundaries far enough from the pipe so that its effect on the background field can be negligible. Without loss of generality, three components of the background magnetic field $\mathbf{B}_b$ in the Cartesian coordinates are set nonzero. The air domain is several times larger than the pipe. All the domains are meshed into tetrahedral and triangular elements with an "Extra fine" meshing configuration. An exemplificative result of the total field norm on transverse and longitudinal slices shows that the magnetic field in the central region of the pipe is uniform. Therefore, the magnetic measurement point is set at the center of the pipe. The axial and radial shielding factors are calculated according to the definition Eq.(1).

In order to compare the differences of the shielding factors calculated by the FEM, IPM, and EM for different LDRs and SDRs, two parameter sets are swept: (1) $D = 200$mm, $L/D = 10$, $\mu_r = 50 \sim 600$, $D/d = 11 \sim 33$, the results are shown in Fig.2**(a)**; (2) $D = 200$mm, $L/D = 2.5 \sim 80$, $D/d = 33$, $\mu_r = 50 \sim 600$, the results are shown in Fig.2**(b)**. In order to utilize small instead of large pipes to carry out magnetic measurement experiments for operation ease, the diameters of the pipes of various SDRs are swept to confirm that the SDR rather than the diameter can change the magnetic shielding factors. The swept parameter set is $D = 80 \sim 762$mm, $L/D = 10$, $D/d = 11 \sim 33$, and $\mu_r = 200$, and the results are shown in Fig.2**(c) and (d)**.

As shown in Fig.2**(a)**, the radial factor λ_r calculated by the FEM is the same as that by the IPM, but differs greatly from that by the EM; λ_r decreases as the permeability μ_r increases and converges to different values for different D/d; Larger D/d leads to larger convergence value. As shown in Fig.2**(b)**, as the pipe become longer, the axial factor λ_a calculated by the EM always converge to 1 even if the permeabilities μ_r are different, which is consistent with the IPM. However, λ_r calculated by the FEM converge to values less than 1, and larger permeability μ_r leads to smaller convergence value. This axial magnetic attenuation is confirmed by the following experiments, and is caused by the magnetic charges at the two ends of the pipe. As shown in Fig.2**(c) and (d)**, when D/d is constant, the axial and radial shielding factors calculated by the three methods are all independent of the pipe diameter. λ_r calculated by the FEM is the same as that by the IPM, but differs greatly from that by the EM.

Based on the above phenomena, three temporary conclusions can be obtained after compared with conventional shielding models [11141521]: First, the radial shielding factor λ_r calculated by the IPM [21] can be accurately verified by the FEM; Second, λ_r is determined by D/d and the permeability μ_r, and is independent of the absolute diameter D, so small size pipes can be adopted for the ease of computation and experimental operation; Third, increasing the pipe length cannot make the axial shielding factor converge to 1 due to the surface and volume magnetic charge densities at the two ends of the pipe, which is different from the IPM [1123] and EM [1415].

The magnetic field **H** in and around magnetized material can be described by the magnetic scalar potential V_m, as $H = -\nabla V_m$. The magnetic potential V_m is determined by the surface charge density σ_m and the volume charge density ρ_m as defined by Eq.(8) [2526]. The magnetization **M** in the material can be directly obtained in the simulation data set. The surface and volume magnetic charge densities of the pipe are then calculated by using Eq.(8). The results are shown in Fig. 3. The magnetic charge densities at the ends is much larger than those in the middle part, and have opposite signs. Independent of the pipe length, the volume and surface magnetic charges at the ends always exist, resulting in a stable existence of the axial component of the demagnetizing fields inside the pipe. The axial magnetic shielding factor

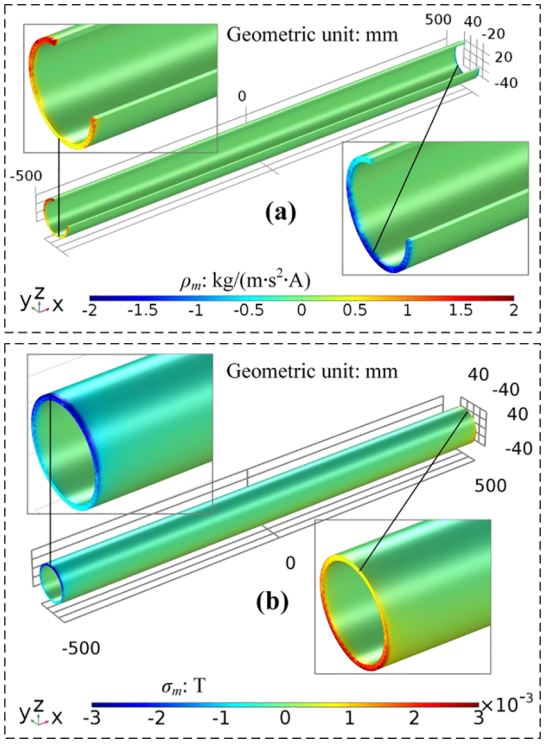

Fig. 3. Volume (a) and surface (b) magnetic charge densities of a pipe.

is therefore less than 1 and independent of the pipe length even if the pipe is long enough.

$$V_m = \frac{1}{4\pi\mu_0}\int_v \frac{-\mu\nabla\cdot M}{\vec{r}}dv + \frac{1}{4\pi\mu_0}\oint_s \frac{\mu_0 M\cdot n}{\vec{r}}ds \\ \frac{1}{4\pi\mu_0}\int_v \frac{\rho_m}{\vec{r}}dv + \frac{1}{4\pi\mu_0}\oint_s \frac{\sigma_m}{\vec{r}}ds \quad (8)$$

2.3. Infinite Pipelines Simulated by Torus Pipes Without Ends

The simulation results above show that no matter how long a pipe is the shielding model cannot transit to an infinite one due to the magnetic charges at the ends. A field pipeline is very long and can be assumed infinite and without ends. Torus pipe has no ends and can be equivalent to an infinite pipeline when the curvature is small enough. The configurations of the torus simulation model are shown in Fig.4**(a)**. The larger the torus radius r is, the closer to a straight pipe the torus is. The magnetic fields in tori with different curvatures are calculated with the FEM by sweeping r, and the magnetic shielding factors are calculated by using Eq.(9). As show in Fig.4**(b)**, the shielding factors converge to the results of the IPM as r increases. The shielding factors converge to constant values when $r > r_0 = 10$m. The torus can be considered straight from a local perspective when $r > r_0 = 10$m and $D = 80$mm.

$$\lambda_r = \frac{B_{1r}}{B_{0r}} = \frac{B_{1x}\cos\phi + B_{1y}\sin\phi}{B_{0x}\cos\phi + B_{0y}\sin\phi} \\ \lambda_a = \frac{B_{1a}}{B_{0a}} = \frac{-B_{1x}\sin\phi + B_{1y}\cos\phi}{-B_{0x}\sin\phi + B_{0y}\cos\phi}. \quad (9)$$

The later experiments demonstrate the magnetic shielding factors of short pipes are randomly distributed, so the overall equivalent permeability μ_r of each section is also randomly distributed. Another torus with the permeability randomly distributed is employed to simulate a field pipeline consisting of a number of short pipes. The torus is with $r = 10$ m, $D = 80$ mm, and $d = 4$ mm, and the section length is 1 m, as shown in Fig.5**(a)**. μ_r is randomly distributed among each section in the range of $(\bar{\mu}_r - \Delta\mu_r, \bar{\mu}_r + \Delta\mu_r)$ with an average of $\bar{\mu}_r$. By taking $\bar{\mu}_r = 112$ and $\Delta\mu_r = 25$, the explicit values of μ_r are plotted as the red curves in Fig.5**(b) and (c)**. As a comparison, a torus of the same size with a

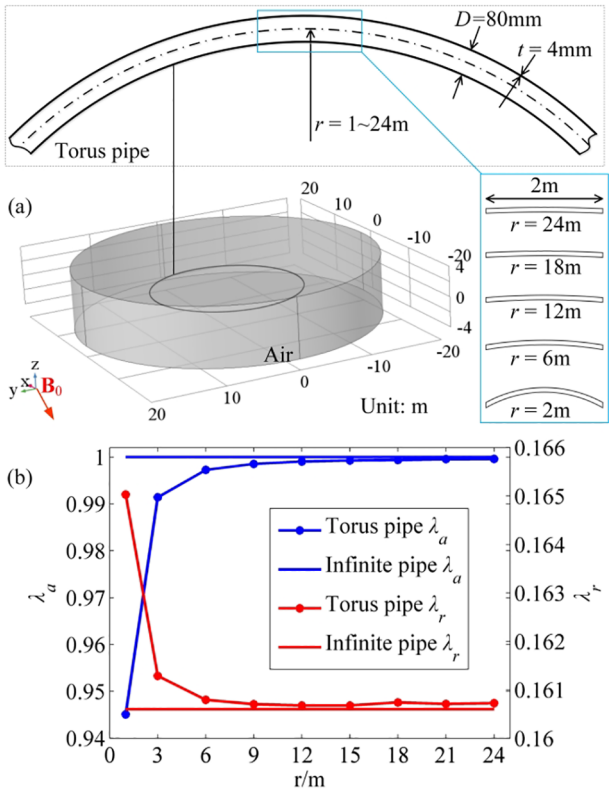

Fig. 4. Magnetic shielding factors for torus pipes to simulate infinite pipelines. (a) Simulation configurations; (b) λ_a and λ_r vs the torus radius r.

uniform permeability $\mu_r = 112$ are also modeled and calculated. The results are shown in Fig.5**(b) and (c)**. The axial shielding factor λ_a inversely varies with the change of μ_r, and randomly fluctuates around the λ_a of the torus pipe with uniform permeability. The radial shielding factor has the same characterization. It can be concluded that the average shielding factors of a pipeline which consists of multiple sections are equal to that of an ideal infinite pipeline with the average permeability of those sections. The field pipeline shielding factors statistically comply with the IPM. Changing the values of $\bar{\mu}_r$ and $\Delta\mu_r$ does not change this conclusion.

Because of random original magnetizations and various permeabilities of each section, the magnetic fields inside pipelines are not uniform even for those adjacent sections in the same direction. However, as the direction of the pipeline changes slow, if the average magnetic components $\overline{B_{1i}}$ inside and the average shielding factors $\overline{\lambda_i}$ of these pipe sections are employed instead, then Eq.(1) can still strictly holds as follows $\overline{\lambda_i} = \overline{B_{1i}}/B_{0i}$, where $i = r$(radial) or a(axial), $\lambda_a = 1$, and λ_r can be calculated by using Eq.(6) or the FEM. There is a clear and predictable mathematical relationship between the magnetic field inside the pipeline and the direction of the pipeline, which can be used to measure the pipeline orientation.

These results above are surprising and promising with regards to pipeline orientation measurement that requires accurate magnetic shielding factors without any approximation. A long pipeline consisting of many sections cannot be accurately modeled via analytical methods like conventional models, while this paper uses torus pipes without ends to successfully mimic a long infinite pipeline. Conventional methods either considers the pipe to be infinitely long [1123] or considers the pipe to be finitely long [1415]; both considerations utilize a uniform magnetic permeability distribution. They focus on the design of large magnetic shielding efficiency [7–9]. It is worth pointing out that, compared with the FEM results that are experimentally verified as follows, none of conventional methods can model the magnetic

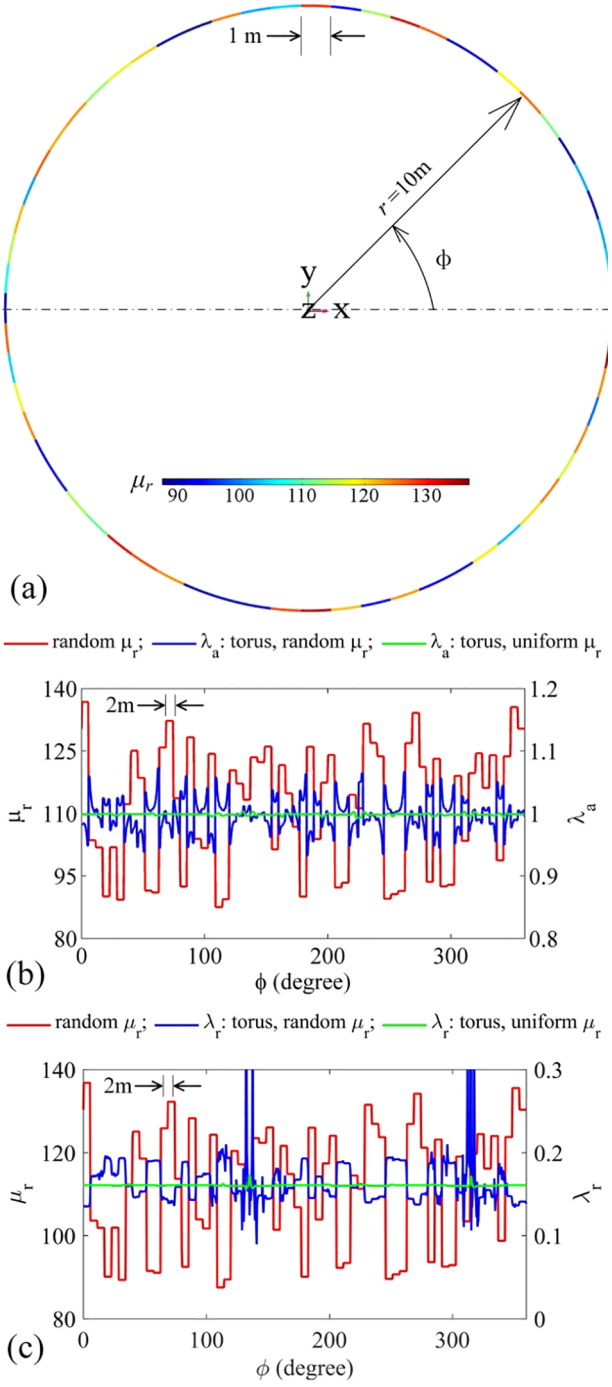

Fig. 5. Magnetic shielding factors for a large thin torus pipe with non-uniform μ_r distributions. (a) Random μ_r distributions with an average of 112; λ_a (b) and λ_r (c) of the torus pipe with random/uniform μ_r.

shielding of a long pipeline, because it consists of many welded short sections. Each section is of finite length and has various magnetic permeabilities due to unpredictable complicated original magnetizations, physical stresses, and thermal treatment processes. The coupling relationship between different segments cannot be expressed either by classical analytical solutions.

3. Experimental verifications for the simulations

In order to verify the above results, the magnetic fields inside steel pipes of different sizes and calculated the shielding factors were measured. Magnetic measurements were carried out on a square in the open air with no disturbing magnetic sources around. The test environment

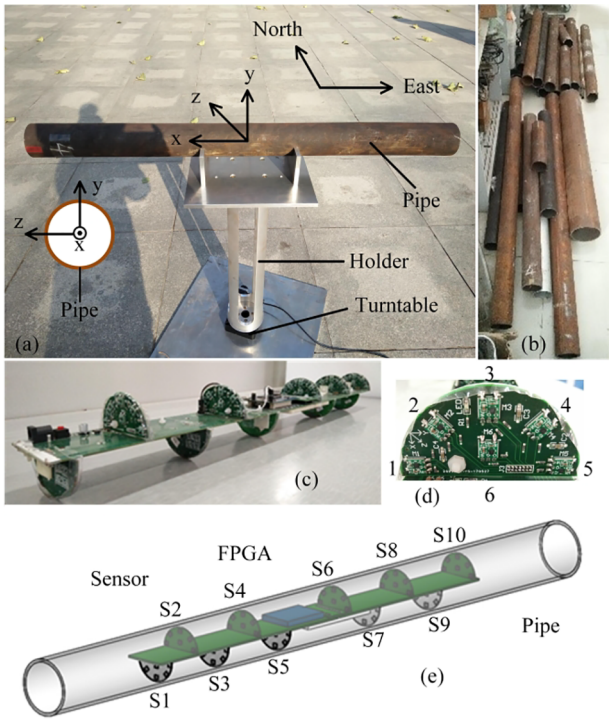

Fig. 6. Experimental apparatus. (a) Non-magnetic rotation platform; (b) Tested pipes; (c) and (d) Magnetic sensor array; (e) Sensor numberings and distributions.

and pipes are shown in Fig. 6 (a) and (b). The measurements are accomplished by a magnetic sensor array consisting of 60 triaxial anisotropic magneto-resistive magnetometers with the model number of LSM303D. The LSM303D contains a 3D digital linear acceleration sensor and a 3D digital magnetic sensor. Its magnetic noise density is 5 mGs/RMS, magnetic sensitivity is 0.080 mGauss/LSB, magnetic measurement range is ± 2 Gauss, and output rate is 50 Sps.

The magnetometers are evenly distributed on 10 cross-section planes, with one sensor located in the center and circularly surrounded by other five on each plane, as shown in Fig.6 **(c)** and **(d)**. The FPGA controller is connected to the base board and the host computer. The FPGA controller synchronously collects the magnetic signals of all the sensors via IIC bus and transmits them to the host computer through USB for saving and display. The magnetic fields measured by the 50 magnetometers on the cylindrical surface are spread out onto a planar graph, as shown in Fig.7 **(a)**. The magnetic field inside the pipe is not uniform. Therefore, in the later analyses, the average of the measuring points in the middle area, as shown in Fig.7 **(b)**, where the fields are more uniform, is used to calculate the shielding factors in order to reduce the calculation error.

During the measurement, the pipe was rotated around the vertical axis for one circle on a turntable, and the shielding factor in each direction can be obtained. For example, one measurement of the axial magnetic component is shown in Fig.8 **(a)**. The DC component is not zero due to the irreversible original magnetization, and needs to be removed. The axial shielding factor is constant except for the middle part, where there are sharp peaks as “zero divided by zero” occurs, as shown in Fig.8 **(b)**. The flat and smooth parts of the axial shielding factor curve are selected and averaged for calculating the final magnetic shielding factor. The calculation procedure of the radial shielding factor is similar. Finally, the axial and radial shielding factors of each pipe are measured and calculated, as shown in Table 1.

As can be seen in Table 1, the shielding factors of these pipes are random and less than 1, which is consistent with the simulation results. The shielding factors are different and disperse even if the pipe sizes are

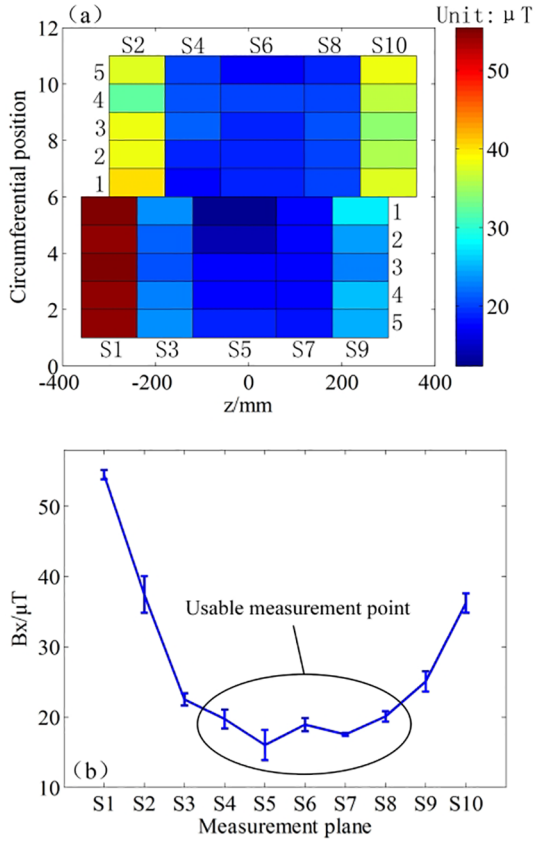

Fig. 7. Measured magnetic fields inside a steel pipe on the (a) cylindrical surface and (b) different cross-sections.

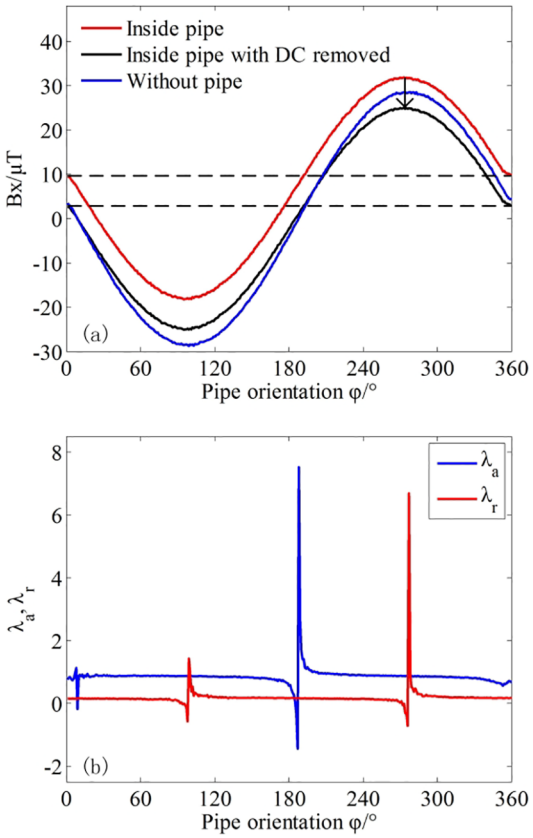

Fig.8. Axial magnetic components (a) and shielding factors (b) vs pipe orientations.

identical. The only reason is that the permeability significantly differs for different pipes due to the variety of the original magnetization during the production process. Therefore, the FEM simulations for all these pipes are carried out to sweep the permeability and search the best-matched permeability value. The calculated factor vs permeability curves and the measurement points based on the IPM are plotted together, as shown in Fig.9. Those discrete points can perfectly overlap those curves. There is always one value for the permeability that can be found to have the measured factor exactly equal to the FEM calculated factor. The simulation results are also confirmed to be correct.

4. Applications of the new shielding model for field pipeline orientations

The magnetic fields inside an on-site annular experimental pipeline were measured by using a SD to verify the correctness of the above conclusions regarding the long pipeline shielding effects and their potential application values for pipeline orientations. The pipeline is buried in an open field and filled with water. A pump pushes the water to continuously flow inside the pipe. The pipeline consists of 9 sections of different directions, as shown in Fig.10**(a)**. The experimental pipeline is made of many sections of short pipes that are welded together. The pipes are made from 20# steel. The pipeline has a total length of 2.5 km, an inner diameter of 175 mm and a wall thickness of 4 mm. As shown in Fig.10**(c) and (d)**, the diameter of the SD is 130 mm and less than the inner diameter of the pipeline. The SD is pushed by the water in the pipeline and can freely roll forward. Magnetometer, accelerometer, batteries, and data recorder are installed inside the SD to record the rotating magnetic and acceleration signals. The magnetometer and accelerometer is LSM303D and its specifications have been listed in Section III. The SD records the magnetic and acceleration signals while rolling forward in the pipeline.

The SD can stably rotate around a fixed axis around which the moment of inertia is the largest among the three. Especially, if mass of the SD is mainly concentrated on a middle plane, the SD can steadily roll around the unique normal axis with strong immunity to sudden disturbance and uncertainty of launch postures. More details can be found in ref. [27]. All the measured data are shown in Fig.11**(a)**. The magnetic intensity noticeably varies inside sections with different directions, and is largest in the north-south direction and smallest in the east-west direction. It can be seen in Fig.11 **(b)** and **(c)** by zooming in the time scale, that the magnetic intensity inside the pipeline is not uniform and the amplitudes are fluctuating. There are many discontinuity points, corresponding to the welding seams. The envelope of the magnetic signals is very similar to the shielding factor distribution of the torus pipe obtained by simulations, as shown in Fig.5, indicating the variety of the permeability and shielding factor.

In order to verify the correctness of the new shielding model of the long pipeline, we calculated and compared the measured and

Table 1
Measured shielding factors of different pipes

Pipe NO.	D (mm)	L(m)	d(mm)	λ_a	λ_r
1	80	0.5	4	0.5871	0.1374
2	80	0.5	4	0.6043	0.1467
3	80	1	4	0.8602	0.1712
4	80	1	4	0.8179	0.1582
5	80	1	4	0.9432	0.1800
6	80	1	4	0.8709	0.1666
7	80	1	4	0.7991	0.1326
8	80	1	4	0.7953	0.1279
9	80	1.5	4	0.9310	0.1389
10	80	2	4	0.9496	0.1716
11	89	1	8.5	0.6322	0.0700
12	89	1.5	8.5	0.7445	0.0775

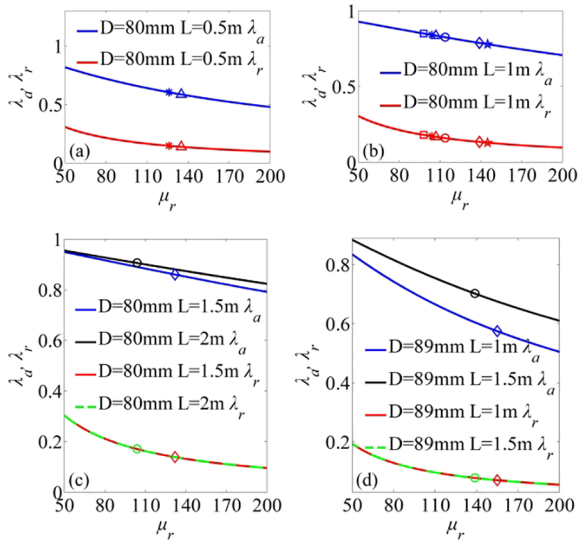

Fig. 9. Sweep μ_r to make the measured λ_a and λ_r equal to that obtained via FEM based simulations.

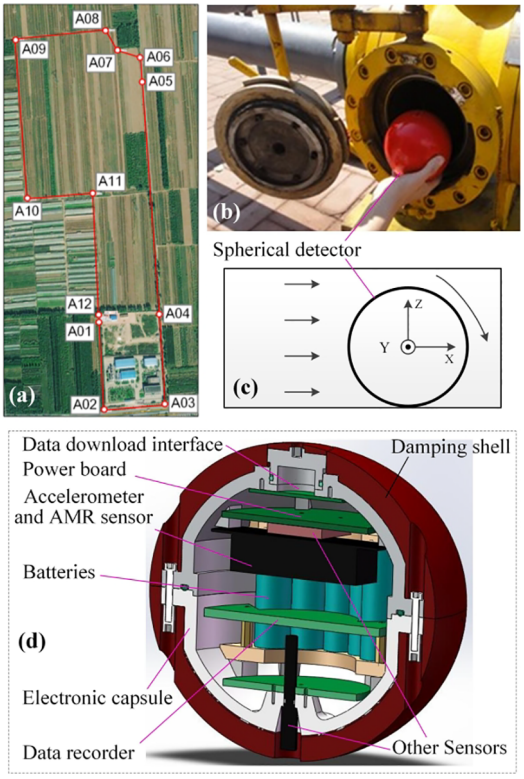

Fig. 10. Field experiments: (a) Distributions of experimental pipelines; (b) Launch and retrieve the SD; (c)The SD is rolling inside the pipeline; (d)Internal structure of the SD.

theoretical magnetic intensity using the equations $|\mathbf{B}_m| = \sqrt{B_{mx}^2 + B_{my}^2 + B_{mz}^2}$ and $|\mathbf{B}_c| = \sqrt{B_{cx}^2 + B_{cy}^2 + B_{cz}^2}$, where the subscript m indicates being measured by the SD and c indicates being calculated by using Eq. (10):

$$\mathbf{B}_c = \begin{pmatrix} \lambda_a & 0 & 0 \\ 0 & \lambda_r & 0 \\ 0 & 0 & \lambda_r \end{pmatrix} \begin{pmatrix} \cos\theta\cos\varphi & \cos\theta sin\varphi & \sin\theta \\ -\sin\varphi & \cos\varphi & 0 \\ -\sin\theta\cos\varphi & -\sin\theta sin\varphi & \cos\theta \end{pmatrix} \mathbf{B}_0. \quad (10)$$

Wherein λ_a is 1; $\mathbf{B}_0$ is the geomagnetic field in the North-East-Down

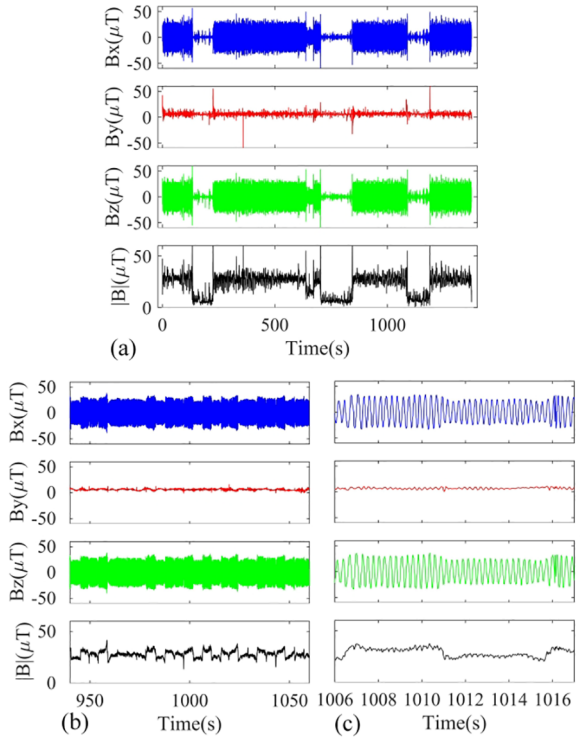

Fig. 11. The magnetic field measured in the pipeline: (a) overall and (b), (c) in detail.

Table 2
Comparison of the measured and calculated magnetic intensities inside each section in different directions

Pipeline NO.	Length(m)	φ(°)	$\lvert\mathbf{B}_c\rvert$(μT)	$\overline{\lvert\mathbf{B}_m\rvert}$(μT)	$\lvert\mathbf{B}_c\rvert - \overline{\lvert\mathbf{B}_m\rvert}$(μT)
A01-A02	249.13	3.27	28.582	28.462	0.12
A02-A03	155.29	91.57	7.032	6.798	0.234
A03-A06	860.75	2.24	27.551	28.188	-0.637
A06-A07	56.42	66.23	15.049	15.669	-0.62
A07-A08	53.21	22.93	26.557	25.639	0.918
A08-A09	236.35	90.57	7.197	7.164	0.033
A09-A10	412.56	2.17	27.549	28.41	-0.861
A10-A11	166.94	91.47	7.047	8.116	-1.069
A11-A12	239.32	3.57	27.589	28.086	-0.497

frame; the inclination θ of the pipeline is 0°, since the experimental pipeline is in the horizontal plane; and the actual azimuths φ of the 9-section pipelines are shown in Table 2. The value of λ_r is determined by sweeping the permeability to minimize the total deviation $\int_{t_1}^{t_2} (|\mathbf{B}_m(t)| - |\mathbf{B}_c(t)|)$ for the section A01-A02, where $\theta = 0°$ and $\varphi = 3.27°$, t_1 and t_2 are the moments when the SD enters and exits the section. The calibrated λ_r is then applied to other eight sections where $|\mathbf{B}_c|$ is calculated by using Eq.(c). $|\mathbf{B}_c|$ in each section and $\overline{|\mathbf{B}_m|}$ that are the averages of measured $|\mathbf{B}_m|$ over each section, are listed together in Table 2. The measured magnetic intensities are very close to the theoretically calculated values, and the maximum deviation is 1μT. This demonstrates an accurate average magnetic shielding model can be obtained when considering the magnetic shielding of many short pipes that are welded together as a whole.

Data subsets of different lengths of the magnetic signals collected in four pipelines with different orientations, A03-A06, A06-A07, A07-A08, A08-A09, are used to calculate the section orientations in order to demonstrate the role of the "average" strategy. The results are plotted in Fig.12. The X-axis caption "Data subset length (~10 m)" means "Length of pipe sections where data subset was collected with unit of 10 m". For all the four pipelines the orientation measurement error is very large

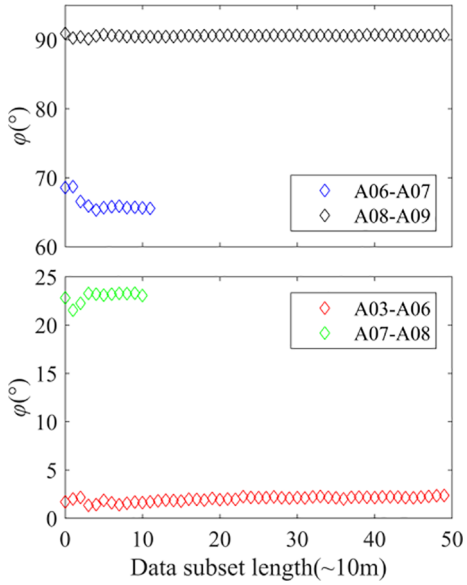

Fig. 12. Role of the "average" strategy in calculating pipeline orientations.

when data subset is short. As the data subset gets longer, the measurement error gets smaller. A long data subset means more sections of pipes are considered as a whole when the shielding factors are used. The permeability of each pipe is random, so the shielding factor of each pipe is also random. When multi-section pipes are welded together, the shielding factor corresponding to their average permeability is equal to the average of their individual shielding factors. The more the sections are, the smaller the error between the two average shielding factors is.

The orientation measurements based on the proposed magnetic shielding model of long pipelines will make a great difference compared with Inertial Navigation System (INS). The INS method with the inner detector as the carrier integrates all the historical acceleration and angular velocity of the carrier in order to calculate the trajectory and orientation of the pipeline axis. The error accumulates and results in positioning divergence and failure if without GPS and geomagnetic navigation. The INS cannot independently work through a long time and distance in the pipeline. The pipeline orientation measurement based on the new magnetic shielding model can be realized by using the magnetic fields and magnetic shielding factors in merely local several pipe sections. The measurement is independent of both the historical running experience of the SD and the pipeline information in other places. As the geomagnetic field is taken as the absolute reference, this orientation measurement method has no risk of divergence, and the precision does not deteriorate with the increase of running time and distance.

5. Conclusions

With the aim of pipeline orientation measurements, this work reveals the magnetic shielding model of long pipelines consisting of many sections with different magnetic permeabilities. FEM based simulations and experiments of the magnetic shielding of short sections, torus pipes, and field long pipelines demonstrate that:

(1) The radial shielding factor λ_r of a finite pipe can be correctly and accurately calculated by both the FEM and the IPM, but cannot by the EM.

(2) The axial shielding factor λ_a is less than 1 because of the magnetic charges at the two ends, and can only be accurately calculated by the FEM. Lengthening a pipe cannot make its shielding model transit to an infinite one.

(3) The average shielding factors of a pipeline which contains multiple sections with different permeabilities are equal to that of an ideal infinite pipeline with the average permeability of those sections. The field pipeline shielding factors statistically comply with the IPM. This is the first time that magnetic shielding of long pipelines aiming for pipeline orientation measurements is analyzed and verified.

The pipeline orientations are then correctly measured via the inner SD based magnetic inspections and calculated by using the averaged magnetic fields and the averaged shielding factors over several sections. The measurement is independent of both the historical running experience of the SD and the pipeline information in other places. As the geomagnetic field is taken as the absolute reference, this orientation measurement method has no risk of divergence over a long time and distance, and the precision does not deteriorate with the increase of running time and distance. The possibility of geomagnetic navigation even in ferromagnetic pipelines is therefore verified.

CRediT authorship contribution statement

Huang Xinjing: Methodology, Funding acquisition, Writing - review & editing, Project administration. **Li Zan:** Methodology, Writing - original draft. **Zhang Yu:** Resources, Project administration. **Xue Yameng:** . **Li Jian:** Funding acquisition, Project administration.

Declaration of Competing Interest

The authors declare that they have no known competing financial interests or personal relationships that could have appeared to influence the work reported in this paper.

Acknowledgments

This work was supported by National Natural Science Foundation of China (Nos 61773283, 61973227 and 51604192).

References

[1] ICNIRP Secretariat, c/o Gunde Ziegelberger, c/o Bundesamt fur Strahlenschutz, Ingolstaedter. Guidelines for limiting exposure to time-varying electric, magnetic, and electromagnetic fields (1 Hz–100 kHz). Health Phys 2010; 99: 818–836.
[2] Davide Bavastro, Aldo Canova, Fabio Freschi, et al., Magnetic Field Mitigation at Power Frequency: Design Principles and Case Studies, IEEE Trans. Ind. Appl. 51 (3) (2015) 2009–2016.
[3] Yong Cui, Haiwen Yuan, Xiao Song, et al., Model, Design and Testing of Field Mill Sensors for Measuring Electric Fields under High-Voltage Direct Current Power Lines, IEEE Trans. Ind. Electron. 65 (1) (2018) 608–615.
[4] Haixia Liu, Kaiming Liu, Zhenjiang Liang, et al. Open-type magnetic shields for optical fiber coil protection with coaxial foil tubes. IEEE Trans. Magn. 2017; 53(5): 6000507 (7 pp.).
[5] Celozzi S, Araneo R, and Lovat G. Electromagnetic Shielding. John Wiley & Sons Inc 2008; 164-199.
[6] Rikitake T. Magnetic and electromagnetic shielding. Reidel Pub. Co. 1987, Dordrecht, Netherlands.
[7] Canova A, Freschi F, Giaccone L, et al. Optimal design of closed multilayer magnetic shields. 2017 International Applied Computational Electromagnetics Society Symposium - Italy, ACES 2017:1-2.
[8] Paperno E, Peliwal S, Romalis M V, et al. Optimum shell separation for closed axial cylindrical magnetic shields. J Appl Phys 2005; 97(10): 10Q104 (3 pp.).
[9] E.A. Burt, C.R. Ekstrom, Optimal three-layer cylindrical magnetic shield sets for scientific applications, Rev. Sci. Instrum. 73 (7) (2002) 2699–2704.
[10] T.J. Sumner, J.M. Pendlebury, K.F. Smith, Convectional magnetic shielding. J. Phys. D, Appl. Phys. 20 (9) (1987) 1095–1101.
[11] A. Mager, Magnetic shields, IEEE Trans. Magn. 6 (1) (1970) 67–75.
[12] D. Azizi, H. Heydari, A. Gholami, Analysis of the shielding effectiveness of several magnetic shields, World Acad. Sci. Eng. Technol. 71 (2010) 151–155.
[13] S. Malkowski, R.Y. Adhikari, J. Boissevain, et al., Overlap Technique for End-Cap Seals on Cylindrical Magnetic Shields, IEEE Trans. Magn. 49 (1) (2013) 651–653.
[14] Mager A. Magnetic Shielding Efficiencies of Cylindrical Shells with Axis Parallel to the Field. J Appl Phys 1968; 39(3): 1914-1914.
[15] Yeqing Hu, Chunsheng Lin, Jianjun Zhou. The Calculation of Magneto-static Shielding Effectiveness of Limited Length Cavity Cylinder Based on the Spheroid Model. Marine Electric & Electronic Technology 2011; 31(8): 45-47, 55.
[16] Xinjing Huang, Guanren Chen, Yu Zhang, et al. Inversion of Magnetic Fields inside Pipelines: Modeling, Validations, and Applications. Struct. Health Monit. 2018; 17(1): 80-90.
[17] Wei Zhao, Xinjing Huang, Shili Chen, et al., A detection system for pipeline direction based on shielded geomagnetic field, Int. J. Press. Vessels Pip. 113 (2014) 10–14.
[18] Huang Xinjing, Chen Guanren, Yu. Zhang, Xu. Li Jian, Chen Shili Tianshu, Inversion

of Magnetic Fields inside Pipelines: Modeling, Validations, and Applications, Struct. Health Monitor. 17 (1) (2018) 80–90.
[19] Shixu Guo, Shili Chen, Xinjing Huang, et al., Design of a Spherical Leak Detector for Submarine Oil Pipelines, Appl. Mech. Mater. 709 (2014) 460–464.
[20] Shixu Guo, Shili Chen, Xinjing Huang, et al., CFD and Experimental Investigations of Drag Force on Spherical Leak Detector in Pipe Flows at High Reynolds Number, Comput. Model. Eng. Sci. 101 (1) (2014) 59–80.
[21] Guo Lin, Zeng Zhoumo, Huang Xinjing, Li Mingze, Feng Hao, Li Jian, Rui Xiaobo, Performance enhancements of the spherical detector for pipeline spanning inspection through posture stabilization, Measurement 165 (2020) 108095.
[22] Guo Lin, Zeng Zhoumo, Huang Xinjing, Li Mingze, Feng Hao, Li Jian, Rui Xiaobo, Low-cost and High-efficiency Method for Detecting Vertical Bends of Subsea Pipelines, IEEE Access 8 (2020) 33926–33933.
[23] Lu. Hongmin, Menglin Xue, Fu. Junmei, Analysis of magneto static shielding effectiveness of the infinite cavity cylinder with magnetic material, Jounal of Xidian University 26 (1) (1999) 80–83.
[24] Q. Bing. Quick Reference of Commonly Used Steel's Magnetic Characteristic Curve. China Machine Press, 2004: 17–18, Beijing, China.
[25] A. Morrish, The Physical Principles of Magnetism, Wiley-IEEE Press (1965) 2–6.
[26] S. Wang, Y. Jia, Equivalent magnetic monopoles model for calculation of magnetic field, Journal of Taiyuan Heavy Machinery Institute 11 (3) (1990) 84–91.
[27] Guo Lin, Zeng Zhoumo, Huang Xinjing, Li Mingze, Feng Hao, Li Jian, Rui Xiaobo. Performance enhancements of the spherical detector for pipeline spanning inspection through posture stabilization.Measurement, 2020, 165: 108095.